Early Response of Hepatocellular Carcinoma to Transcatheter Arterial Chemoembolization: Choline Levels and MR Diffusion Constants—Initial Experience[1]

Chiao-Yun Chen, MD
Chun-Wei Li, PhD
Yu-Ting Kuo, MD
Twei-Shiun Jaw, MD
Ding-Kwo Wu, MD
Jo-Chi Jao, PhD
Jui-Sheng Hsu, MD, PhD
Gin-Chung Liu, MD

Purpose: To prospectively investigate the apparent diffusion coefficient (ADC) and choline levels measured at hydrogen 1 (^{1}H) magnetic resonance (MR) spectroscopy, to monitor therapeutic responses of hepatocellular carcinoma (HCC) to transcatheter arterial chemoembolization (TACE).

Materials and Methods: Institutional review board approval was obtained, and all patients and control subjects provided informed consent. Histologically proved large HCCs (>3 cm in diameter) were evaluated in 20 patients (16 men and four women; mean age, 59 years; range, 34–80 years) before TACE and 2–3 days after TACE. A control group of eight adults (five men and three women; mean age, 43 years; range, 24–76 years) with normal livers was examined by using the same protocol. Hepatic choline levels were measured by means of an external phantom replacement method, quantifying the peak at 3.2 ppm at ^{1}H MR spectroscopy. ADCs were measured for all lesions. A Wilcoxon rank sum test was used to compare absolute choline concentrations and ADCs at baseline between HCCs and normal liver parenchyma. Changes in choline levels and ADCs in the tumors before and after TACE were analyzed by using the Wilcoxon signed rank test.

Results: The median preoperative choline level in patients with HCC (measured in 18 of the 20 patients) was 4.0 mmol/L (range, 0.0–17.2 mmol/L), which was significantly higher than that in patients with normal livers ($n = 8$) (median, 1.6 mmol/L; range, 0.0–2.1 mmol/L; $P < .01$). Among 18 patients with HCC, choline levels decreased significantly from before TACE to after TACE ($P < .01$). A significant increase in ADC from before TACE to after TACE in the 20 patients with HCC was also found ($P < .01$).

Conclusion: Hepatic choline levels and ADCs may allow monitoring of therapeutic responses of HCC to TACE although larger, more definitive and quantitative studies with clinical end points are needed.

[1] From the Department of Medical Imaging (C.Y.C., Y.T.K., T.S.J., D.K.W., J.S.H., G.C.L.) and School of Medical Radiation Technology (C.W.L., J.C.J.), Kaohsiung Medical University, 100 Tz You 1st Road, Kaohsiung 807, Taiwan. Received January 2, 2005; revision requested March 10; revision received April 11; accepted May 19; final version accepted July 5. **Address correspondence to** G.C.L. (e-mail: *gcliu@kmu.edu.tw*).

Transcatheter arterial chemoembolization (TACE) is a well-accepted means of treatment in patients with unresectable hepatocellular carcinoma (HCC), because TACE provides substantial survival benefits (1–5). Although evaluating the effectiveness of TACE is critical in determining the success of treatment and would help to guide subsequent therapeutic planning, there is no absolutely reliable imaging method for monitoring the early response to this treatment method. Good iodized oil retention at computed tomography (CT) is associated with substantial prolongation of median survival of the patient but does not indicate complete tumor necrosis, nor is it correlated with the size or extent of the necrotic area. On dynamic CT studies, hyperattenuating iodized oil impairs assessment of residual tumor enhancement. Iodized oil causes variable signal intensity changes on unenhanced magnetic resonance (MR) images, and it is difficult to detect accurately (6,7). Enhancing areas in the embolization site on gadolinium-enhanced MR images presumably represent viable tumor but could also result from posttreatment granulation tissue (8). Lang et al (9) reported that even gadolinium-enhanced MR imaging cannot unfailingly enable distinction between viable and dead tumor cells. Unenhanced ultrasonography (US) cannot aid differentiation of viable tumor from dead tumor. Contrast material–enhanced harmonic US has been used successfully to detect intratumoral vascularity in HCC after TACE, but it is not helpful in lesions that do not show hypervascularity on US studies obtained before TACE (10).

In vivo hydrogen 1 (^{1}H) MR spectroscopy has proved valuable in the diagnosis of tumors in the brain (11–15), prostate (16,17), breast (18,19), and uterine cervix (20). ^{1}H MR spectroscopy is also useful in the evaluation of treatment responses in malignant tumors of the head and neck (21), as well as in breast cancers (22). In the liver, ^{1}H MR spectroscopy has been used to evaluate diffuse hepatic disease (23–27). Phosphorous 31 MR spectroscopy has been used in the assessment of the effectiveness of chemoembolization treatment (28), but no reliable pathognomonic metabolic correlate of therapeutic efficacy has been found following chemoembolization. To our knowledge, our research group published the first article quantifying metabolic changes at ^{1}H MR spectroscopy (by using a 3.0-T MR imager) and correlating them with therapeutic responses of HCCs after TACE by a choline-lipid ratio (29). However, we determined that the lipid value after TACE was proportionally increased because the iodized oil (Lipiodol Ultra Fluide; Laboratoires Guerbet, Aulnay-Sous-Bois, France) used for TACE has a substantial lipoid component. Therefore, we designed a new strategy—measuring absolute choline concentrations by using ^{1}H MR spectroscopy (30).

Apparent diffusion coefficient (ADC) measurement is currently the best imaging method for in vivo quantification of diffusion. A primary application of this approach has been the evaluation of brain lesions, including those from acute ischemic stroke, intracranial tumors, trauma, and demyelinating disease (15,31–33).

In the liver, ADC values have been used to differentiate hepatic abscess from cystic or necrotic tumors (34) and to differentiate benign from malignant hepatic masses (35,36). To our knowledge, however, there have been no studies on the use of diffusion-weighted MR imaging to *(a)* evaluate the therapeutic effects of TACE on large HCCs after treatment, *(b)* reveal pathophysiologic changes, and *(c)* differentiate viable from dead tumor cells. Thus, the purpose of our study was to prospectively investigate ADC, as well as choline levels measured at ^{1}H MR spectroscopy, to monitor therapeutic responses of HCC to TACE in patients.

Materials and Methods

Patients

The protocol in our study was approved by our institutional review board, and informed consent was obtained from all patients and control subjects. From March 2002 to March 2004, 20 consecutive patients (16 men and four women; mean age, 59 years; age range, 34–80 years) with large HCCs (mean diameter, 9.5 cm; diameter range, 5.0–17.2 cm) histologically confirmed at percutaneous biopsy or aspiration cytologic evaluation were prospectively evaluated at diffusion-weighted MR imaging and ^{1}H MR spectroscopy before TACE and 2–3 days after TACE. The time elapsed between the MR examination and the TACE procedure was 1 or 2 days. All patients had undergone US and biphasic contrast-enhanced CT. Nonenhanced CT, to depict the distribution of iodized oil (Lipiodol Ultra Fluide; Laboratoires Guerbet), was also performed 2–3 days after TACE. To establish a control group, we used the same protocols to evaluate eight patients (five men and three women; mean age, 43 years; age range, 24–76 years) who underwent an abdominal MR examination to evaluate nonhepatic problems; these control subjects had normal findings at liver imaging and liver function tests and showed no clinical evidence of liver disease.

MR Imaging

All patients were examined by using a 3.0-T MR imager (Signa VH$_3$, GE Medical Systems, Milwaukee, Wis) with a 40 mT/m maximum gradient capability and built-in body coil. All patients under-

Published online before print
10.1148/radiol.2392042202

Radiology 2006; 239:448–456

Abbreviations:
ADC = apparent diffusion coefficient
HCC = hepatocellular carcinoma
TACE = transcatheter arterial chemoembolization

Author contributions:
Guarantors of integrity of entire study, C.Y.C., G.C.L.; study concepts/study design or data acquisition or data analysis/interpretation, all authors; manuscript drafting or manuscript revision for important intellectual content, all authors; manuscript final version approval, all authors; literature research, C.Y.C., C.W.L., J.S.H., G.C.L.; clinical studies, C.Y.C., C.W.L., Y.T.K., T.S.J., D.K.W., J.C.J., G.C.L.; statistical analysis, J.S.H.; and manuscript editing, C.Y.C., C.W.L., Y.T.K., G.C.L.

Authors stated no financial relationship to disclose.

went transverse fast spin-echo fat-saturated T2-weighted MR imaging. MR imaging was performed in all patients with HCC both before TACE and 2–3 days after TACE.

MR Spectroscopic Evaluation

Conventional MR imaging for routine diagnostic purposes was followed with ^{1}H MR spectroscopy. Patients were examined in the supine position. Shallow, regular breathing was allowed during MR spectroscopic data acquisition, and the breathing skills were taught beforehand. Localizing the image for spectroscopic data acquisition was first performed by using a spin-echo sequence (repetition time msec/echo time msec, 350/30; image matrix, 256 × 256; one signal acquired) to indicate the selection of the voxel of interest (2 × 2 × 3 cm). For localization, spectra were obtained by using a point-resolved spin-echo sequence. Water suppression was accomplished by using three preceding chemical shift–selective saturation pulses; the bandwidth of each of these pulses was 60 Hz. The field homogeneity was optimized automatically over the selected voxel of interest by observing the water signal intensity. The following acquisition parameters were used: repetition time sec/echo time msec, 1.5/30; 128 acquisitions; four dummy measurements; spectral width, 2500 Hz; and 2048 data points. For phase correction of metabolite spectra, 16 additional acquisitions were collected without water suppression in the sequence. The location of the voxel of interest was determined by a radiologist (C.Y.C.) with more than 7 years of experience in gastrointestinal and hepatobiliary MR imaging. On the basis of previous images, the largest solid portion of the HCC was selected. For each patient, we compared images for the same location before and after TACE. In the control group, MR spectroscopy was performed in the middle portion of the right hepatic lobe, thus avoiding the great vessels.

After acquisition, data were processed by using the MR spectroscopic analysis package provided by the manufacturer (SAGE 7.1; GE Medical Systems). The raw data were zero-filled once, apodized with a 5-Hz Gaussian filter, Fourier transformed, and phase and baseline corrected. Marquardt curve fitting was performed by using a Gaussian line shape to calculate the area under the peak. MR spectroscopic data were analyzed by a single medical physicist (C.W.L.) with more than 10 years of experience in MR spectroscopic analysis. The physicist was blinded to clinical data and imaging findings.

Absolute metabolite concentrations were calculated by using the choline peak and a standard calibration phantom as a reference. The average value of the area of the choline peak, which was derived from a long-term signal intensity stability test recorded over the course of 8 months, was used as the reference (I_{ref}). The coefficients of variance of the detected intensity for the choline signal was calculated to be 6%.

By using the peak in the HCC spectrum, we calculated the concentration of choline by using the following equation:

$$C_m = C_{\text{ref}} \cdot \frac{I_m \cdot f_{\text{T1}(m)} \cdot f_{\text{T2}(m)}/(f_L \cdot n_m \cdot V_m)}{I_{\text{ref}} \cdot f_{\text{T1(ref)}} \cdot f_{\text{T2(ref)}}/(n_{\text{ref}} \cdot V_{\text{ref}})},$$

where C_m and C_{ref} are the concentrations of the metabolite in the tissue and choline in the standard phantom, respectively; I_m and I_{ref} are the localized signal integrals from the liver and the standard phantom, respectively; f_L is a factor that takes into account the variation of coil loadings by patients and the phantom; and the parameters $f_{\text{T1}(m)}$ and $f_{\text{T1(ref)}}$ are correction factors for T1 effects on the partial saturation of metabolite signals and choline signal in the standard phantom, respectively: $f_{\text{T1}} = 1/(1 - e^{-\text{TR}/\text{T1}})$, where TR indicates repetition time. In patients with HCC, we used the mean saturation factor from four HCC tumors to correct this factor because of the long experimental T1 measurement time. The saturation factor was calculated by using two repetition time values of 1.5 and 8.0 seconds. The parameters $f_{\text{T2}(m)}$ and $f_{\text{T2(ref)}}$ are correction factors for the effect of T2 on the specific length of echo time (TE) of metabolite signals and choline signal in the standard phantom, respectively: $f_{\text{T2}} = 1/e^{-\text{TE}/\text{T2}}$. In patients with HCC, we used the mean T2 value from four HCC tumors to correct this factor. The values of T2 for choline in the liver tumors were estimated by using four echo time values (30, 90, 150, and 300 msec); the values of T2 were extracted by fitting the data as a function of echo time to a monoexponential model. The variable n_m is the number of protons per molecule contributing to the metabolite signal of the tissue; n_{ref} is the choline compound in the standard calibration phantom ($n_{\text{ref}} = 9$); and V_m and V_{ref} are the selected localization volumes of the tissue and the standard calibration phantom, respectively (30).

Loading effects between the standard phantom and the in vivo liver studies were investigated in the eight control subjects by using a cylindrical bottle of water (diameter, 6 cm; height, 14 cm) that was placed close to the control subjects. A standard coil-loading correction factor from the mean value of control subjects was used to correct for the coil-loading effect.

Diffusion-weighted MR Imaging

Diffusion-weighted MR images were obtained in 18-second breath-hold periods by using a transverse spin-echo echo-planar sequence (repetition time msec/echo time msec, 4000/6.1; gradient strength, 40 mT/m; matrix size, 64 × 140; section thickness, 8 mm; intersection gap, 0.8 mm; one signal acquired; field of view, 360 mm).

Diffusion-weighted MR images and ADC maps were acquired by using b values of 0 and 500 sec/mm^2 applied in the z direction. Quantitative ADC maps were calculated by using commercially available software and an imaging workstation (Functool and AW 4.0; GE Medical Systems). ADC values were measured by a radiologist (G.C.L.) with more than 15 years of experience in gastrointestinal and hepatobiliary MR imaging and more than 4 years of experience in diffusion-weighted MR imaging of livers. We measured ADC values by placing a region of interest over the entire area of the treated mass, section

by section in thicknesses of 10 mm, and avoided torsion and artifact regions. The number of imaging sections of the tumors in all patients ranged from four to 12 depending on the tumor size. The final ADC value in each case was determined by means of the average of all sections obtained. The region of interest of ADC values included the entire lesion because of the heterogeneous nature of the lesions.

Chemoembolization Technique

An 18-gauge single-wall needle was used to access the right common femoral artery by using the Seldinger technique. A 5-F vascular sheath was placed into the right common femoral artery over a 0.035-inch guidewire (Glidewire; Terumo Medical, Somerset, NJ). With fluoroscopic guidance, a 4-F glide Yashiro catheter (Cordis, Miami, Fla) was advanced into the aortic arch, formed, and then used to select the celiac axis. The catheter was advanced over the guidewire into the desired hepatic artery branch, depending on the tumor location. Chemoembolization drugs were mixed with a 2:1 ratio of epirubicin (30–50 mg) (Pharmorubicin; Pharmacia & Upjohn, Milan, Italy), mitomycin (6–10 mg) (Mitomycin-C; Kyowa Hakko Kogyo, Tokyo, Japan), and nonionic contrast material (6–30 mL) (Ultravist; Schering, Berlin, Germany) to iodized oil (3–15 mL) (Lipiodol Ultra Fluide; Laboratoires Guerbet), the dose of which depended on the tumor size. After slow effusion of the chemoembolization drugs and gelatin sponge particles (1 mm^3) (Gelfoam; Upjohn, Kalamazoo, Mich), complete embolization of the feeding hepatic artery was achieved. The TACE procedures were performed by an interventional radiologist (D.K.W.) with 18 years of experience.

All patients underwent nonenhanced CT after TACE. The CT and angiographic images were prospectively read by two radiologists (Y.T.K., T.S.J.) with 8 and 15 years of experience, respectively, in abdominal and interventional image interpretation. They evaluated the success of TACE procedures independently. Differences in assessment were resolved by means of discussion and consensus. Evaluation criteria included the following: *(a)* good (50%–74%) iodized oil retention in the tumor, *(b)* low attenuation ischemic or edematous change within the tumor, and *(c)* embolization through the correct segmental or subsegmental feeding arteries.

Statistical Analysis

The median and range of choline levels and ADC values in patients with HCC and in the control subjects were described. Because of the small sample size in this study, nonparametric statistics were used. A Wilcoxon rank sum test was used to compare absolute choline levels and ADC values at baseline between HCCs and normal liver parenchyma. Among the patients with HCC, the Wilcoxon signed rank test was used to compare the differences in choline levels and ADC values before and after TACE. Differences were considered significant when P values were less than .05.

Results

^{1}H MR Spectroscopy

Of the 20 patients with HCC who were included in our study, two (patients 1 and 2) underwent two follow-up imaging studies and a second TACE procedure because of tumor recurrence. In two patients (patients 19 and 20), studies showed poor spectroscopic resolution, both before and after TACE, because of massive ascites and severe motion artifacts. Patients with ascites had studies with more motion artifacts than did patients without ascites because of dyspnea and discomfort, and this motion tends to ruin the spectral data; therefore, choline levels could be evaluated in only 18 of the 20 patients with HCC.

The median preoperative absolute choline level in 18 patients with HCC was 4.0 mmol/L (range, 0.0–17.2 mmol/L), which was significantly higher than that in normal liver parenchyma (median, 1.6 mmol/L; range, 0.0–2.1 mmol/L; $P < .01$, Wilcoxon rank sum test) (Table 1). Among the 18 patients evaluated, median absolute choline concentrations before and after TACE were 4.0 mmol/L (range, 0.0–17.2 mmol/L) and 0.4 mmol/L (range, 0.0–3.5 mmol/L), respectively. Differences (after TACE minus before TACE) of absolute choline levels were significantly different from zero (Table 2, Fig 1) ($P < .01$, Wilcoxon signed rank test). Choline resonance at 3.2 ppm on the ^{1}H MR spectroscopic images decreased after TACE treatment in all cases except one (Fig 2). Lipoid resonance at 0.9–1.4 ppm increased after TACE because of the embolization agent iodized oil deposition (Fig 3).

Diffusion-weighted MR Images

Diffusion-weighted images were successfully obtained for all 20 patients. The median ADC value among the 20 patients with HCC was 1.56 mm^2/sec (range, 1.12–2.31 mm^2/sec), which was not significantly different from that among those with normal liver parenchyma (median, 1.67 mm^2/sec; range, 2.08–1.46 mm^2/sec; $P > .05$, Wilcoxon rank sum test) (Table 1). Among the 20 patients with HCC, median ADC values before and after TACE were 1.56 mm^2/sec (range, 1.12–2.31 mm^2/sec) and 2.09 mm^2/sec (range, 1.47–2.70 mm^2/sec), respectively. Differences (after

Table 1

Absolute Choline Levels and ADC Values between HCC before TACE and Normal Liver Parenchyma

Parameter	HCC before TACE*	Normal Liver ($n = 8$)	P Value†
Median choline level (mmol/L)	4.0 (0.0–17.2)	1.6 (0.0–2.1)	<.01
Median ADC ([mm^2/sec] × 10^{-3})	1.56 (1.12–2.31)	1.67 (2.08–1.46)	>.05

Note.—Data in parentheses are the ranges.

* Choline level was evaluated in 18 patients, and ADC was evaluated in 20 patients.

† Wilcoxon rank sum test.

TACE minus before TACE) in ADC values were significantly different from zero (Table 3, Fig 4). ($P < .01$, Wilcoxon signed rank test). The difference in diffusion before TACE versus after TACE was clearly demonstrated on ADC map images. Tumor necrosis was seen as regions of bright signal intensity on ADC maps, which indicated free diffusion of water molecules, whereas viable tumor was seen as regions of low signal intensity on ADC maps, which indicated limited diffusion (Fig 5a, 5b). However, the signal intensity changes on the T2-weighted MR images before and after TACE were not obvious (Fig 5c, 5d).

Two patients underwent repeated follow-up imaging examinations because of tumor recurrence. For these patients, ^{1}H MR spectroscopic images and diffusion-weighted MR images showed patterns of changes in choline and ADC that were similar to before and after the first TACE procedure: Choline concentrations had returned to high levels before the second TACE procedure; choline levels decrease after the second TACE procedure; ADC values increased from before the second TACE procedure to after the second procedure. At statistical analysis, we excluded the results of the additional (second) procedure in each of these patients.

Discussion

The usefulness of ^{1}H MR spectroscopy in evaluating responses to treatment has been reported for malignancies of the head and neck, breast, uterine cervix, and prostate (21,37,38). Jagannathan et al (22) reported that among 67 patients with breast cancer undergoing neoadjuvant chemotherapy, absence of or reduction in choline level was observed in 89% of patients. In our study, 94% of the patients with HCC had decreased choline concentrations after TACE treatment (ie, 17 of 18 patients in whom choline concentration was evaluated). At ^{1}H MR spectroscopy, choline and its derivatives are thought to represent important constituents in the phospholipid metabolism of cell membranes (39). Elevation of the choline peak is thought to represent increased membrane phospholipids biosynthesis and is also thought to be an active marker for cellular proliferation and/or cell density that occurs with the evolution and progression of cancer (40,41).

In our in vivo ^{1}H MR spectroscopy study, we found a strong relationship between the signal intensity at ^{1}H MR spectroscopy and the presence of a malignant HCC. All HCCs except one (in patient 3) displayed a baseline choline peak that was higher than control values; almost all displayed a reduction in the choline peak after TACE treatment. Histologically, the one HCC that failed to display an elevated choline peak showed fibrotic degeneration without malignant cells at the first biopsy procedure, with the specimen taken randomly at the tumor site, and a few malignant cells at the second biopsy procedure, with the specimen taken specifically at the periphery of the enhanced tumoral part. Angiograms (Fig 2a) showed hypovascularity of the tumor, and T2-weighted MR images (Fig 2b) demonstrated central high and peripheral low signal intensities owing to necrotic degeneration and fibrotic content in the tumor. The findings of nonsignificant choline changes without a high choline peak before and after TACE in this patient (Fig 2c) might thus be a reflection of reduced cellularity and of decreased cell proliferation in the tumor caused by excessive necrosis, degeneration, and fibrotic content. We do not believe that this was due to inconsistent positioning of the MR spectroscopic region of interest, because an experienced radiologist (C.Y.C.) consistently selected the same lesion site, thus ensuring a constant voxel-of-interest site for the two MR spectroscopic studies obtained before and after TACE. Therefore, this is not a false-negative case.

One patient (patient 2) underwent two follow-up imaging examinations owing to tumor recurrence. At the second follow-up examination, we selected voxels of interest at two sites, the tumoral necrotic part and the true recurrent tumoral part, to observe their differences. The ^{1}H MR spectroscopic study ob-

Figure 1

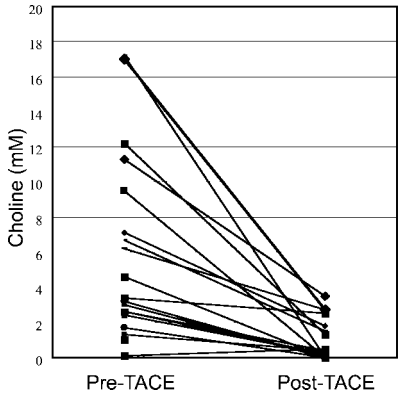

Figure 1: Graph of changes in absolute choline concentration at ^{1}H MR spectroscopy shows significant decline in absolute choline concentration after TACE among 18 patients who underwent TACE, with the exception of only one patient, in whom a hypovascular tumor with necrotic and fibrotic content was shown at histologic evaluation.

Table 2

Difference in Absolute Choline Levels before and after TACE in 18 Patients

Patient No.	Choline Level (mmol/L) Before TACE	After TACE	Difference (mmol/L)*
1	11.3	3.5	−7.8
2	2.6	0.4	−2.2
3	0	0.5	0.5
4	1.7	0	−1.7
5	2.6	0	−2.6
6	17.2	0	−17.2
7	6.2	2.7	−3.5
8	17.0	2.7	−14.3
9	9.5	0	−9.5
10	2.4	0	−2.4
11	4.6	0	−4.6
12	12.2	1.3	−10.9
13	3.2	0	−3.2
14	3.4	2.5	−0.9
15	6.7	1.5	−5.2
16	1.3	0.4	−0.9
17	7.1	1.8	−5.3
18	3.0	0	−3.0
Median	4.0	0.4	−3.4

* $P < .001$ for all (Wilcoxon signed rank test).

tained before TACE showed an elevated choline peak in the recurrent part of the tumor but no elevation in choline peak in the necrotic part of the tumor. After TACE, the lack of a definite choline peak at either site suggested that the treated necrotic HCC remained at a lower choline concentration and that TACE effectively decreased the choline concentration in the recurrent part of the tumor. These re-elevations of choline levels caused by tumor recurrence and re-reductions due to a second TACE procedure support our finding that HCC elevates and TACE reduces hepatic choline levels.

The detection of a signal from the liver at ^{1}H MR spectroscopy is challenging. Physiologic motion due to breathing and heartbeat may increase background noise and further hinder the detection of small amounts of metabolites within the tumors, especially in the left hepatic lobe and extreme end of the right hepatic lobe. In our study, two cases were considered technical failures owing to severe motion, which reduced signal-to-noise ratios. Therefore, further development of new MR techniques, such as the breath-hold technique with a phase-array torso coil, are needed for more precise examinations (42). Furthermore, quantification of choline-related compounds with the ratio method by using an internal standard such as water or lipid is difficult because the background of liver tissue is highly variable. Iodized oil infusion used in TACE may increase lipid concentrations. Therefore, to prevent iodized oil contamination we used the external phantom replacement method (30) to quantify the absolute choline concentration and evaluate metabolic changes after TACE.

Although the standard deviation for choline levels in normal liver was quite large in our study, we cannot make comparisons since, to our knowledge, ours is the first report of hepatic choline by using MR. We believe that the large standard deviation was due to the motion effect of breathing. We estimated the precision of this method of quantification by using white matter of brain ($n = 5$). The coefficient of variation was 25%.

In normal liver, Lim et al (43) found that the ^{1}H MR spectrum of the liver showed that lipid compounds peak at 0.9–1.4 ppm and choline compounds peak at 3.2 ppm. Our study revealed similar findings; a choline resonance was present in normal livers. However, the mean absolute concentration was relatively low. In our study, among both control subjects and patients with HCC, the absolute choline concentration varied from 1.0 to 17.2 mmol/L, and this could perhaps be related to different phases of cell growth or to different tumor grades with different choline contents.

In our study, we found no difference in results between normal liver and HCC. All the large HCCs showed different degrees of necrosis with typical MR imaging findings of high signal intensity on T2-weighted MR images, low signal intensity on T1-weighted MR images, and no enhancement on MR images obtained after administration of contrast material. This may be due to the HCCs with necrotic portions causing greater extracellular free water content. In our study, all patients had increased ADC values at diffusion-weighted MR imaging performed after TACE. Taouli et al (36) reported that ADC values can be used to differentiate between benign and malignant hepatic lesions because

Figure 2

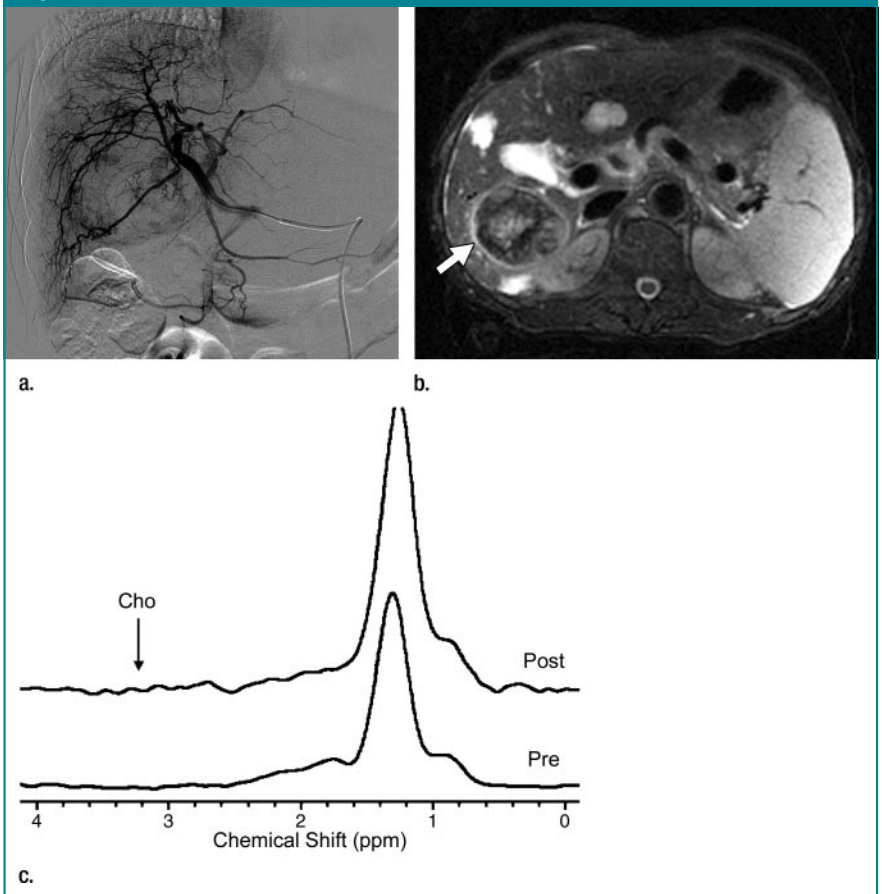

Figure 2: Images in 69-year-old man with HCC at posterior-inferior segment of the right hepatic lobe demonstrate the one case with no decrease in choline concentration after TACE. **(a)** Posteroanterior angiogram of right hepatic artery reveals hypovascular HCC at segment VI, where TACE is performed. **(b)** Transverse fast spin-echo fat-saturated T2-weighted MR image (10 000/100; flip angle, 90°) shows a hypointense tumor with central high-signal-intensity content (arrow). **(c)** Before TACE *(Pre)* and after TACE *(Post)*, the ^{1}H MR spectrum shows no significant choline resonance at 3.2 ppm.

Figure 3

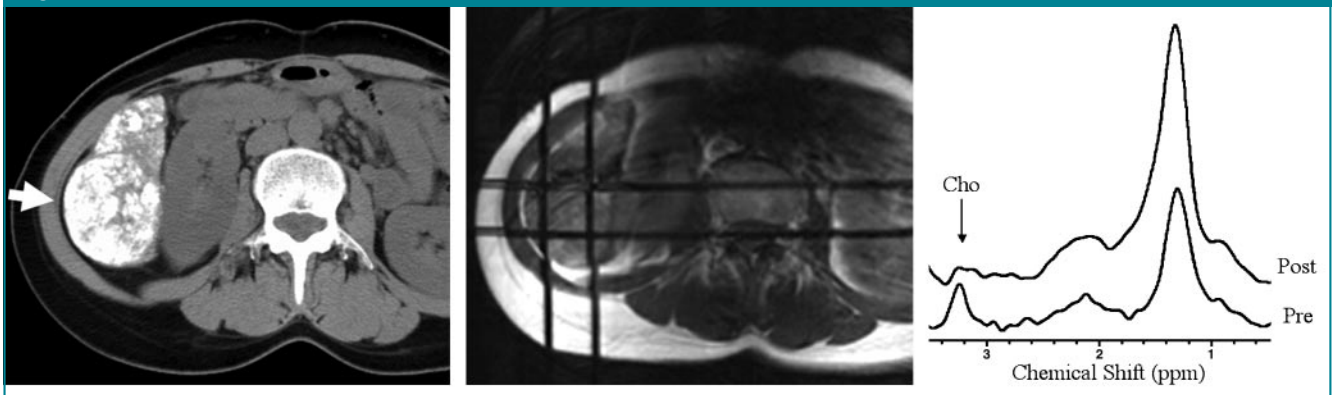

a. b. c.

Figure 3: Images in 56-year-old woman with HCC at the postinferior segment of the right hepatic lobe demonstrate spectrum of ^{1}H MR spectroscopy and changes in choline and lipid content after TACE in a typical case. **(a)** Nonenhanced transverse CT scan 2 days after TACE reveals complete (≥75%) iodized oil retention in the tumor (arrow). **(b)** Localized MR image (350/30) shows location of the voxel of interest in the tumor, with the same location before and after TACE. **(c)** ^{1}H MR spectrum shows significant choline resonance decrease (arrow, at 3.2 ppm) before TACE *(Pre)* and after TACE *(Post)*. The lipid resonance (0.9–1.4 ppm) displays an increase after TACE caused by iodized oil infusion during TACE.

of the low ADC values in malignant tumors (including HCCs). Kim et al (44) affirmed that ADC values of the necrotic portion of tumors are high. In our study, we could not differentiate HCCs from normal liver by using ADC values; this is possibly because the large HCCs may have been contaminated by variable necrotic parts.

Our study had technical limitations. First, we used a single, relatively large voxel of 2 × 2 × 3 cm in our MR spectroscopy study. Contamination error was therefore possible. Also, because of the large voxel, we could not definitely distinguish or sample the necrotic part from the viable part in tumors after TACE. Hence, development of multivoxel two- or three-dimensional chemical shift imaging with breath-hold MR spectroscopy would be the best method for future evaluation. Second, although we used a 3.0-T MR imager to increase signal-to-noise ratio, image distortions and susceptibility artifacts were unavoidable to some degree. Therefore, a definite differentiation between necrotic parts and viable parts after TACE is difficult because of the lower spatial resolution and the greater heterogeneity of the HCCs. Findings in recent studies have shown that new imaging sequences can improve image quality and may be useful in future investigations (45). Diffusion-weighted single-shot echo-planar imaging was combined with sensitivity encoding to further increase the potential of echo-planar imaging for diffusion imaging. No ghost or aliasing artifacts were discernible, and echo planar–related image distortions were markedly diminished. Chemical shift ar-

Table 3

Difference in ADC Values before and after TACE in 20 Patients

Patient No.	ADC ([mm^2/sec] × 10^{-3}) Before TACE	ADC ([mm^2/sec] × 10^{-3}) After TACE	Difference* ([mm^2/sec] × 10^{-3})
1	2.14	2.34	0.20
2	2.10	2.31	0.21
3	1.23	1.47	0.24
4	1.61	1.89	0.27
5	2.35	2.70	0.35
6	1.55	2.23	0.68
7	1.53	1.80	0.27
8	1.39	1.87	0.48
9	1.76	2.09	0.33
10	1.38	2.27	0.89
11	1.31	2.24	0.93
12	1.64	1.81	0.17
13	1.64	1.94	0.30
14	1.54	1.74	0.20
15	1.29	2.08	0.79
16	1.56	2.19	0.63
17	1.12	1.65	0.53
18	1.52	1.92	0.40
19	2.14	2.64	0.50
20	1.81	2.32	0.51
Median	1.56	2.09	0.38

* $P < .001$ for all (Wilcoxon signed rank test).

Figure 4

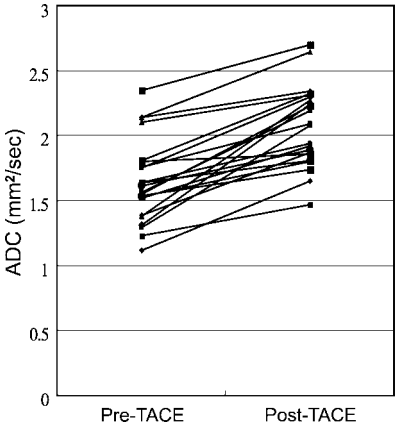

Figure 4: Graph of change in ADC values in HCCs after TACE. These data showed a statistically significant increase in all cases because of increased water diffusion after embolization.

tifacts and eddy current–induced image warping were still present, although to a markedly smaller extent. Because of the faster k-space reversal, this novel technique is able to reduce typical echo-planar imaging artifacts and increase spatial resolution while simultaneously remaining insensitive to bulk motion (46).

Third, the patient population in this study was relatively small, so further studies with a larger number of patients are needed to reach a firmer conclusion. Fourth, we were unable to obtain images and pathologic correlations of the hepatic lesions after chemoembolization because most of these patients did not undergo surgery (they were not candidates). Also, follow-up data on patient outcomes such as survival were not available.

In conclusion, in vivo ^{1}H MR spectroscopic changes that show hepatic choline levels may be a useful strategy for the evaluation of therapeutic effectiveness of the response of large HCCs to TACE. Diffusion-weighted MR images that show ADC values may be useful in assessing the early therapeutic responses of large HCCs after TACE by depicting tumor necrosis with increasing ADC values and by means of signal intensity changes on diffusion-weighted MR images and ADC maps. However, ADC values cannot contribute to the initial differential diagnosis because of the large tumor size, which may be contaminated by tumor necrosis. A combination of ^{1}H MR spectroscopy (for choline) and diffusion-weighted MR imaging (for ADC) might turn out to be useful for assessing the early therapeutic responses in large HCCs after TACE and for guiding patient care. Further refinements of MR techniques would promote its usefulness for assessment of smaller lesions.

Figure 5

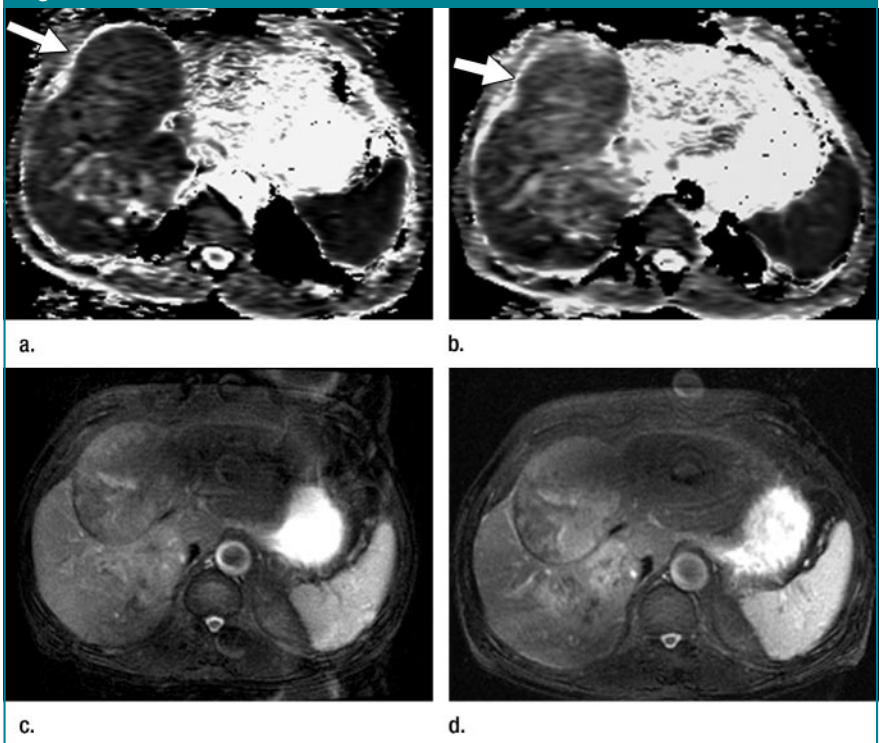

Figure 5: MR images in 34-year-old woman with HCC at anterior segment of the right hepatic lobe show correlation of signal intensity change between ADC mapping and traditional MR images. **(a, b)** Transverse spin-echo echo-planar (4000/6.1) images at *b* value of 500 sec/mm^2 obtained **(a)** before and **(b)** after TACE show heterogeneous hypointense mass before TACE (arrow) and significantly increased signal intensity after TACE (arrow), owing to tumor necrosis and increased extracellular free water content. **(c, d)** Transverse fast spin-echo fat-saturated T2-weighted images (1000/100; flip angle, 90°) **(c)** before and **(d)** after TACE show a mild increase in signal intensity of the tumor mass after TACE.

Acknowledgments: The authors gratefully acknowledge the assistance of Yen-Yu Chiu, BS, and Feng-O Sheu, BS, for MR technical support.

References

1. Colombo M. Nonpercutaneous therapies of hepatocellular carcinoma. Hepatogastroenterology 2001;48:25–28.

2. Ramsey DE, Kernagis LY, Soulen MC, Geschwind JF. Chemoembolization of hepatocellular carcinoma. J Vasc Interv Radiol 2002;13(suppl 2): S211–S221.

3. Solomon B, Soulen MC, Baum RA, Haskal ZJ, Shlansky-Goldberg RD, Cope C. Chemoembolization of hepatocellular carcinoma with cisplatin, doxorubicin, mitomycin-C, ethiodol, and polyvinyl alcohol: prospective evaluation of response and survival in a U.S. population. J Vasc Interv Radiol 1999;10:793–798.

4. Vogl TJ, Trapp M, Schroeder H, et al. Transarterial chemoembolization for hepatocellular carcinoma: volumetric and morphologic CT criteria for assessment of prognosis and therapeutic success—results from a liver transplantation center. Radiology 2000;214:349–357.

5. Ngan H, Lai CL, Fan ST, Lai EC, Yuen WK, Tso WK. Transcatheter arterial chemoembolization in inoperable hepatocellular carcinoma: 4-year follow-up. J Vasc Interv Radiol 1996;7:419–425.

6. Imaeda T, Yamawaki Y, Seki M, et al. Lipiodol retention and massive necrosis after lipiodol-chemoembolization of hepatocellular carcinoma: correlation between computed tomography and histopathology. Cardiovasc Intervent Radiol 1993; 16:209–213.

7. Ito K, Honjo K, Fujita T, et al. Therapeutic efficacy of transcatheter arterial chemoembolization for hepatocellular carcinoma: MRI and pathology. J Comput Assist Tomogr 1995;19:198–203.
8. De Santis M, Alborino S, Tartoni PL, Torricelli P, Casolo A, Romagnoli R. Effects of lipiodol retention on MRI signal intensity from hepatocellular carcinoma and surrounding liver treated by chemoembolization. Eur Radiol 1997;7:10–16.
9. Lang P, Wendland MF, Saeed M, et al. Osteogenic sarcoma: noninvasive in vivo assessment of tumor necrosis with diffusion-weighted MR imaging. Radiology 1998;206:227–235.
10. Ding H, Kudo M, Onda H, et al. Evaluation of posttreatment response of hepatocellular carcinoma with contrast-enhanced coded phase-inversion harmonic US: comparison with dynamic CT. Radiology 2001;221:721–730.
11. Murphy M, Loosemore A, Clifton AG, et al. The contribution of proton magnetic resonance spectroscopy (1HMRS) to clinical brain tumour diagnosis. Br J Neurosurg 2002;16:329–334.
12. Law M, Cha S, Knopp EA, Johnson G, Arnett J, Litt AW. High-grade gliomas and solitary metastases: differentiation by using perfusion and proton spectroscopic MR imaging. Radiology 2002;222:715–721.
13. Moller-Hartmann W, Herminghaus S, Krings T, et al. Clinical application of proton magnetic resonance spectroscopy in the diagnosis of intracranial mass lesions. Neuroradiology 2002;44:371–381.
14. Burtscher IM, Holtas S. Proton MR spectroscopy in clinical routine. J Magn Reson Imaging 2001; 13:560–567.
15. Bulakbasi N, Kocaoglu M, Ors F, Tayfun C, Ucoz T. Combination of single-voxel proton MR spectroscopy and apparent diffusion coefficient calculation in the evaluation of common brain tumors. AJNR Am J Neuroradiol 2003;24:225–233.
16. Scheidler J, Hricak H, Vigneron DB, et al. Prostate cancer: localization with three-dimensional proton MR spectroscopic imaging—clinicopathologic study. Radiology 1999;213:473–480.
17. Yu KK, Scheidler J, Hricak H, et al. Prostate cancer: prediction of extracapsular extension with endorectal MR imaging and three-dimensional proton MR spectroscopic imaging. Radiology 1999;213:481–488.
18. Yeung DK, Cheung HS, Tse GM. Human breast lesions: characterization with contrast-enhanced in vivo proton MR spectroscopy—initial results. Radiology 2001;220:40–46.
19. Gribbestad IS, Singstad TE, Nilsen G, et al. In vivo 1H MRS of normal breast and breast tumors using a dedicated double breast coil. J Magn Reson Imaging 1998;8:1191–1197.
20. Allen JR, Prost RW, Griffith OW, Erickson SJ, Erickson BA. In vivo proton (H1) magnetic resonance spectroscopy for cervical carcinoma. Am J Clin Oncol 2001;24:522–529.
21. Mukherji SK, Gerstle RJ. In vitro 1H MR spectroscopy of squamous cell carcinoma of the extracranial head and neck. Neuroimaging Clin N Am 1998;8:835–847.
22. Jagannathan NR, Kumar M, Seenu V, et al. Evaluation of total choline from in-vivo volume localized proton MR spectroscopy and its response to neoadjuvant chemotherapy in locally advanced breast cancer. Br J Cancer 2001;84:1016–1022.
23. Longo R, Ricci C, Masutti F, et al. Fatty infiltration of the liver: quantification by 1H localized magnetic resonance spectroscopy and comparison with computed tomography. Invest Radiol 1993; 28:297–302.
24. Cho SG, Kim MY, Kim HJ, et al. Chronic hepatitis: in vivo proton MR spectroscopic evaluation of the liver and correlation with histopathologic findings. Radiology 2001;221:740–746.
25. Lim AK, Patel N, Hamilton G, Hajnal JV, Goldin RD, Taylor-Robinson SD. The relationship of in vivo 31P MR spectroscopy to histology in chronic hepatitis C. Hepatology 2003;37:788–794.
26. Menon DK, Sargentoni J, Taylor-Robinson SD, et al. Effect of functional grade and etiology on in vivo hepatic phosphorus-31 magnetic resonance spectroscopy in cirrhosis: biochemical basis of spectral appearances. Hepatology 1995;21:417–427.
27. Taylor-Robinson SD, Sargentoni J, Bell JD, et al. In vivo and in vitro hepatic 31P magnetic resonance spectroscopy and electron microscopy of the cirrhotic liver. Liver 1997;17:198–209.
28. Schilling A, Gewiese B, Berger G, et al. Liver tumors: follow-up with P-31 MR spectroscopy after local chemotherapy and chemoembolization. Radiology 1992;182:887–890.
29. Kuo YT, Li CW, Chen CY, Jao J, Wu DK, Liu GC. In vivo proton magnetic resonance spectroscopy of large focal hepatic lesions and metabolite change of hepatocellular carcinoma before and after transcatheter arterial chemoembolization using 3.0-T MR scanner. J Magn Reson Imaging 2004;19:598–604.
30. Li CW, Kuo YC, Chen CY, Kuo YT. Quantification of human hepatic tumors in vivo by phantom replacement method of proton MR Spectroscopy at 3 Tesla. Magn Reson Med (in press).
31. Bammer R, Stollberger R, Augustin M, et al. Diffusion-weighted imaging with navigated interleaved echo-planar imaging and a conventional gradient system. Radiology 1999;211:799–806.
32. Lutsep HL, Albers GW, DeCrespigny A, Kamat GN, Marks MP, Moseley ME. Clinical utility of diffusion-weighted magnetic resonance imaging in the assessment of ischemic stroke. Ann Neurol 1997;41:574–580.
33. Schaefer PW, Grant PE, Gonzalez RG. Diffusion-weighted MR imaging of the brain. Radiology 2000;217:331–345.
34. Chan JH, Tsui EY, Luk SH, et al. Diffusion-weighted MR imaging of the liver: distinguishing hepatic abscess from cystic or necrotic tumor. Abdom Imaging 2001;26:161–165.
35. Namimoto T, Yamashita Y, Sumi S, Tang Y, Takahashi M. Focal liver masses: characterization with diffusion-weighted echo-planar MR imaging. Radiology 1997;204:739–744.
36. Taouli B, Vilgrain V, Dumont E, Daire JL, Fan B, Menu Y. Evaluation of liver diffusion isotropy and characterization of focal hepatic lesions with two single-shot echo-planar MR imaging sequences: prospective study in 66 patients. Radiology 2003; 226:71–78.
37. Bizzi A, Movsas B, Tedeschi G, et al. Response of non-Hodgkin lymphoma to radiation therapy: early and long-term assessment with H-1 MR spectroscopic imaging. Radiology 1995;194:271–276.
38. Schwarz AJ, Maisey NR, Collins DJ, Cunningham D, Huddart R, Leach MO. Early in vivo detection of metabolic response: a pilot study of 1H MR spectroscopy in extracranial lymphoma and germ cell tumours. Br J Radiol 2002;75:959–966.
39. Dixon RM. NMR studies of phospholipid metabolism in hepatic lymphoma. NMR Biomed 1998;11: 370–379.
40. Ruiz-Cabello J, Cohen JS. Phospholipid metabolites as indicators of cancer cell function. NMR Biomed 1992;5:226–233.
41. Mukherji SK, Schiro S, Castillo M, Kwock L, Muller KE, Blackstock W. Proton MR spectroscopy of squamous cell carcinoma of the extracranial head and neck: in vitro and in vivo studies. AJNR Am J Neuroradiol 1997;18:1057–1072.
42. Katz-Brull R, Rofsky NM, Lenkinski RE. Breath-hold abdominal and thoracic proton MR spectroscopy at 3T. Magn Reson Med 2003;50:461–467.
43. Lim AK, Hamilton G, Patel N, Bell JD, Taylor-Robinson SD. ^{1}H MR spectroscopy in the evaluation of the severity of chronic liver disease [letter]. Radiology 2003;226:288–289.
44. Kim YJ, Chang KH, Song IC, et al. Brain abscess and necrotic or cystic brain tumor: discrimination with signal intensity on diffusion-weighted MR imaging. AJR Am J Roentgenol 1998;171:1487–1490.
45. Bammer R, Keeling SL, Augustin M, et al. Improved diffusion-weighted single-shot echo-planar imaging (EPI) in stroke using sensitivity encoding (SENSE). Magn Reson Med 2001;46: 548–554.
46. Pruessmann KP, Weiger M, Scheidegger MB, Boesiger P. SENSE: sensitivity encoding for fast MRI. Magn Reson Med 1999;42:952–962.